Fluorescent Crystals

International Edition: DOI: 10.1002/anie.201508210
German Edition: DOI: 10.1002/ange.201508210

Stimuli-Responsive Reversible Fluorescence Switching in a Crystalline Donor–Acceptor Mixture Film: Mixed Stack Charge-Transfer Emission versus Segregated Stack Monomer Emission

*Sang Kyu Park, Illhun Cho, Johannes Gierschner, Jin Hong Kim, Jong H. Kim, Ji Eon Kwon, Oh Kyu Kwon, Dong Ryeol Whang, Jung-Hwa Park, Byeong-Kwan An, and Soo Young Park**

Abstract: *We report on a molecularly tailored 1:1 donor–acceptor (D-A) charge-transfer (CT) cocrystal that manifests strongly red-shifted CT luminescence characteristics, as well as noteworthy reconfigurable self-assembling behaviors. A loosely packed molecular organization is obtained as a consequence of the noncentrosymmetric chemical structure of molecule* ***A1****, which gives rise to considerable free volume and weak intermolecular interactions. The stacking features of the CT complex result in an external stimuli-responsive molecular stacking reorganization between the mixed and demixed phases of the D-A pair. Accordingly, high-contrast fluorescence switching (red↔blue) is realized on the basis of the strong alternation of the electronic properties between the mixed and demixed phases. A combination of structural, spectroscopic, and computational studies reveal the underlying mechanism of this stimuli-responsive behavior.*

Multi-color photoluminescence (PL) switching on the basis of structural perturbation for organic π-conjugated materials has recently attracted enormous research interest and paved the way toward developing future applications such as optical recording and sensors.[1] Various materials have been devised showing actively controllable PL characteristics triggered by external stimuli, such as thermal stimuli, mechanical stimuli, and solvent vapor treatment. However, structural reorganizations are enabled by utilizing rather limited and specific intermolecular interaction motifs (for example, local dipole alignment,[1b] aurophilic interactions,[1c] and conformational changes)[1d] or by introducing co-/disassembling stacking modulators.[1e] Moreover, in many cases PL changes are limited to rather small energetic shifts, which are based on transitions between excitonic and excimeric interactions. Furthermore, it is not feasible to predict the existence of multiple phases of the organic material itself and its luminescence alternations during the structural transformation. Accordingly, at this stage, we desire an intuitive and straightforward guideline for both controlling and predicting luminescence changes based on anticipated structural rearrangements.

Multi-component charge-transfer (CT) complexes comprised of intermolecular donor–acceptor (D-A) pairs can resolve this issue. In these systems, predictable mixed stacking structures are provided, governed by the Coulombic interaction induced from the large energetic offset between donors and acceptors.[2] This mixed arrangement, in turn, gives rise to distinguished emission energies originating from localized frontier molecular orbitals (MO), that is, the highest occupied MO (HOMO) at the donor, and the lowest unoccupied MO (LUMO) at the acceptor, respectively; this enables the pronounced bathochromic shift of emission compared to the individual D/A materials. However, detrimental non-radiative deactivation of the CT state should be resolved; furthermore, facile phase transition between the mixed D-A phase (CT) and the demixed phase (individual D/A) will promote multi-color fluorescence switching based on the D-A complex.[3,4] Among the recent advances in highly emissive D-A complex systems,[5] we further gave attention to the CT system consisting of the isometrically tailored distyrylbenzene-based D-A pair.[6] This D-A pair exhibited strong red PL and low internal conversion rates through establishing densely packed stacking structure; however, the intended loosely packed molecular arrangement is necessary for a stimuli-responsive feature. Therefore, it is expected that a high-contrast, multi-color switching system can be realized by using similar isometric chromophores for which **A1** has a noncentrosymmetric design for an attenuated intermolecular interaction network. In this context, the PL switching between mixed and demixed (that is, narcissistic self-sorting) phases is allowed;[1e,7] meanwhile, the PL is defined by its CT and its individual D/A state during structural reorganization.

Herein, we propose a strategy for establishing high-contrast, reversible PL switching media based on stimuli-responsive CT complexes. Facile stacking control between the mixed D-A CT complex and the demixed individual D/A phases can be attained by implanting the noncentrosymmetric **A1** to obtain the intended loosely packed structure, which can be characterized by distinct free volume and relatively weak intermolecular interactions (see Figure 1a for chemical

[*] S. K. Park, I. Cho, J. H. Kim, Dr. J. H. Kim, Dr. J. E. Kwon, O. K. Kwon, D. R. Whang, J.-H. Park, Prof. S. Y. Park
Center for Supramolecular Optoelectronic Materials
Department of Materials Science and Engineering
Seoul National University, ENG 445
Seoul 151-744 (Korea)
E-mail: parksy@snu.ac.kr
Dr. J. Gierschner
Madrid Institute for Advanced Studies, IMDEA Nanoscience
C/Faraday 9, Ciudad Universitaria de Cantoblanco
28049 Madrid (Spain)
Prof. B.-K. An
Department of Chemistry, The Catholic University of Korea
Bucheon-si, Geyonggi-do 420-753 (Korea)

Supporting information for this article is available on the WWW under http://dx.doi.org/10.1002/anie.201508210.

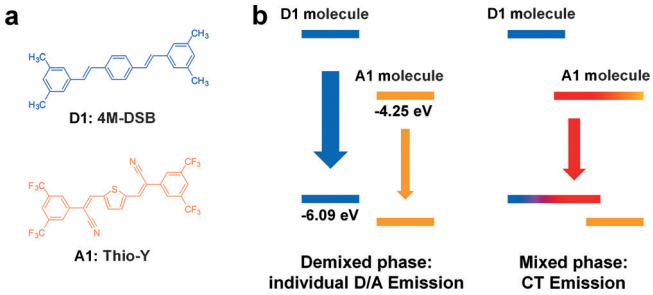

Figure 1. a) Chemical structures of donor (**D1**: 4M-DSB) and acceptor (**A1**: Thio-Y). b) Frontier molecular orbital diagrams of mixed and demixed phases.

structures of **D1** and **A1**). On the basis of the large energetic shift of the S_0-S_1 transition during the phase change (Figure 1b), we expect to achieve a programmable PL memory system that is controlled by polarity- or proticity-dependent solvent vapor annealing (SVA), as well as thermal/mechanical stimuli. In turn, these stimuli greatly modulate the intermolecular interactions based on electrostatic CT and H-bonding interaction motifs. An in-depth understanding of the unique PL switching mechanism induced from dynamic structural changes can be accomplished through a precise correlation of the chemical, structural, optical, and thermal properties.

The distyrylbenzene-based **D1** (4M-DSB) and dicyanodistyrylthiophene-based **A1** (Thio-Y) materials were prepared by simple synthetic procedures, as described previously.[6,8] The CT phenomenon of this D-A system can be observed through UV/Vis absorption and PL spectroscopy (Figure 2 and Table 1). To avoid artifacts such as high optical density in a single crystal, we measured solid-state absorption

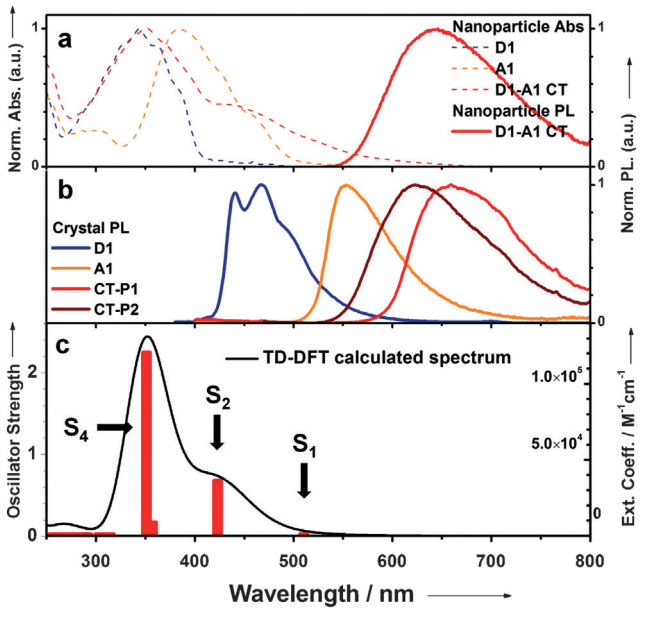

Figure 2. a) Normalized UV/Vis absorption of **D1**, **A1**, **D1-A1** nanoparticles, and normalized PL spectra of **D1-A1** nanoparticles. b) Normalized PL spectra of **D1**, **A1**, CT-P1, and CT-P2 single crystals. c) Calculated absorption spectrum of **D1-A1** dimer by TD-DFT.

Table 1: Optical properties of CT complex and constituent compounds in the solid state: absorption (λ_{abs}) and emission (λ_{em}) wavelengths, absolute quantum yields (Φ_F), intensity-weighted average fluorescence lifetimes (τ_F), radiative rates (k_r), and non-radiative rates (k_{nr}).

	D1	A1	CT-P1	CT-P2
λ_{abs} [nm]	343	384	353, 444, 525[a]	[b]
λ_{em} [nm]	467	553	660	622
Φ_F	0.88	0.19	0.03	0.08
τ_F [ns]	1.47	2.65	3.62	3.10
k_r [ns^{-1}]	0.601	0.070	0.009	0.026
k_{nr} [ns^{-1}]	0.079	0.307	0.267	0.296

[a] CT band observed from nanoparticle suspension absorption spectrum. [b] Cannot be recorded owing to the high optical density, because CT-P2 only exists in the powder/crystal form. Absorption (λ_{abs}) and emission (λ_{em}) wavelengths, absolute quantum yields (Φ_F), intensity-weighted average fluorescence lifetimes (τ_F), radiative rates (k_r), and non-radiative rates (k_{nr}).

using nanoparticle representing solid-state CT. The **D1-A1** nanoparticle absorption reveals a new weak band at around 525 nm, which gives rise to PL at 660 nm. This low-lying state is well correlated with the (reported) experimental gap between the HOMO (**D1**) and LUMO (**A1**) energies (that is, −6.09 and −4.25 eV, respectively);[6] this is theoretically assigned to the $S_0 \rightarrow S_1$ transition, which has a pronounced CT character (Figure 2; Supporting Information, Figure S1, Tables S1 and S2). The broad PL of the cocrystal and nanoparticle shows a strong bathochromic shift against the individual solid-state PL spectra of **D1** (467 nm) and **A1** (553 nm) crystals. This suggests significant potential for use in multi-color PL switching systems for which (de-)mixed phases can be controlled by external stimuli.

We envisage that the noncentrosymmetric design of **A1** establishes the basis for programmable structure/PL switching. The molecular arrangement in the CT cocrystal was analyzed by single-crystal XRD (SC-XRD), which showed a dimer-pair brick-wall-like geometry with a 1:1 **D1-A1** mixed stack within its triclinic unit cell (Figure 3; Supporting Information, Table S3).[9] The solved structure revealed two important structural features: weak intermolecular interactions and distinct free volume in the lattice. Upon solving the molecular stacking structure, it was clarified that inclusion of other components (most probably, solvent) occurred in the crystal structure, as analyzed from residual electron density other than **D1** and **A1** with 1:1 stoichiometry. This solvent inclusion was further confirmed by thermogravimetry analysis (TGA) and NMR spectroscopy. However, owing to the inevitable disorder of the solvent, the solvent-included structure (named CT-P1) could be roughly understood.[9] The result, however, well reflects free volume, which acts as a solvent molecular inclusion site, provided by the curved molecular shape of **A1** (Figure 3c). Furthermore, the loosely packed state was confirmed on the basis of a relatively large π-plane distance of approximately 3.5 Å and moderately weak -CN-induced intermolecular interactions (for example, the -CN···HC- interaction between two **A1** molecules, with 2 hydrogen bonds per molecule and a distance of 2.6 Å; Figure 3b).

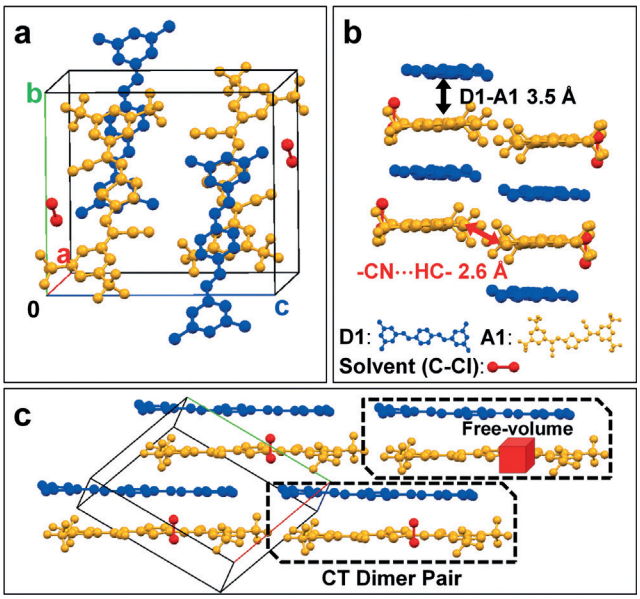

Figure 3. a–c) Molecular arrangement of CT-P1 (solvent-included structure) from SC-XRD. **D1**: blue molecule; **A1**: yellow molecule; and solvent (C-Cl): red molecule. b) Roll-angle view with information of the **D1-A1** π-π distance (black arrow) and the **A1-A1** -CN···HC- distance (red arrow). c) Slip-angle view showing dimer-pair brick-wall geometry. Black dotted box: **D1-A1** dimer pair; red cube: lattice free volume.

In combination with the solvent-included form (CT-P1), we further found that the solvent-excluded form (CT-P2) can also be grown, and can give rise to emission property alternations (CT-P1: $\lambda_{em} = 660$ nm, $\Phi_F = 3.2\,\%$; CT-P2: $\lambda_{em} = 622$ nm, $\Phi_F = 8.1\,\%$; see the Supporting Information, Figures S2 and S3). Those structural features well reflect our intended sparsely packed molecular arrangement compared to the reported CT based on the centrosymmetric dicyanodistyrylbenzene-based acceptor,[6] which facilitates phase alteration in response to multiple stimuli, and thus leads to high-contrast luminescence switching behavior.

For a qualitative understanding of solvent property effects, and also for a demonstration of optical memory capabilities, we performed SVA using a wide range of solvents, which were selected based on their proticity and empirical polarity values, $E_T(30)$.[10,11] $E_T(30)$ values of the solvents are listed in Figure 4.[10,11] The appropriately attenu-

Figure 4. Digital images of CT spin-coated films taken under 365 nm UV irradiation.

ated intermolecular interaction and its adequate free-volume indeed gave rise to superior external-stimuli responsive features. The pristine **D1-A1** spin-coated film shows PL resembling that of the CT-P1 crystal ($\lambda_{em} = 658$ nm, black open/solid diamond spectra in Figure 5a); however, it exhibits abrupt solvent-dependent biphasic phase alteration during

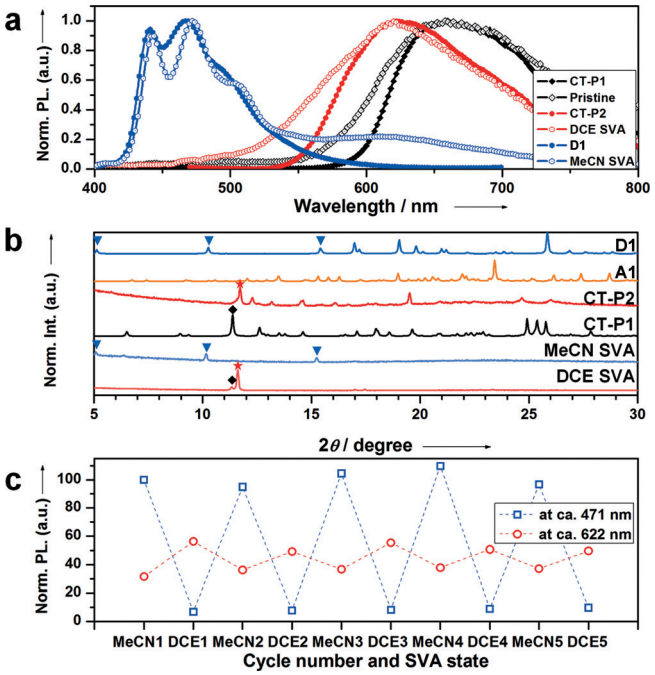

Figure 5. a) Normalized PL spectra of pristine (black open diamond), DCE-SVA (red open circle), and MeCN-SVA (blue open hexagon) spin-coated films. Each state is compared with CT-P1 (black diamond), CT-P2 (red circle), and **D1** (blue hexagon), respectively. b) XRD data of **D1**, **A1**, CT-P1, CT-P2 single crystals, and spin-coated films of the DCE- and MeCN-SVA states. c) The blue triangle, black diamond, and red star indicate characteristic peaks of **D1**, CT-P1, and CT-P2, respectively. The relative PL intensity transition during repetitive SVA processes using MeCN and DCE at ca. 471 nm (blue open square), and ca. 622 nm (red open circle).

the SVA procedure (Figures 4 and 5a).[8] As visualized in the fluorescence images and spectra, the nonpolar solvents and polar protic solvents give rise to red emission ($\lambda_{em} = 619$ nm from 1,2-dichloroethane (DCE) SVA, which resembles the PL of CT-P2, red open/solid circle spectra of Figure 5a). On the other hand, the polar aprotic solvent results in blue fluorescence (for example, acetonitrile (MeCN), $\lambda_{em} =$ 472 nm, blue open/solid hexagon spectra of Figure 5a). This can be attributed to the mixed **D1-A1** CT formation that occurs when using the nonpolar or polar protic solvents; however, blue emission in the latter (polar aprotic) is greatly affected by the self-assembled structure of **D1** in the demixed phase. The out-of-plane XRD pattern of each film state supports this reconfiguration-based PL switching behavior, that is, the appearance of the CT-P2 characteristic peaks (red star) in the DCE SVA case, compared with the appearance of lamellar **D1** peaks (blue triangle) in the MeCN SVA case (Figure 5b). Notably, the peculiar stacking features also rendered reversibility, showing consecutive switching behavior between the moderate red PL of the mixed CT phase (DCE SVA, λ_{em} of ca. 622 nm) and the bright blue PL of the demixed phase (MeCN SVA, λ_{em} of ca. 472 nm; Figures 5c, S4, and S5).

The biphasic SVA dependence of molecular reorganization can be well explained by the nature of the intermolecular interactions and the role of the solvent.[12] The binding affinity

of **D-A** CT complexes with respect to solvent polarity is usually governed either by i) electrostatic interactions governing CT complexation, or by ii) CT complexation driven by the solvophobic effect. Electrostatic CT and H-bonding interactions become severely interrupted by a polar solvent owing to its ionic character in the former case;[13] in the latter, however, those interactions can be promoted by polar protic solvents on the basis of strong H-bonding-induced solvent–solvent interactions.[14] The current CT system exceptionally follows both principles, showing the polarity criterion of approximately $E_T(30) = 41–42$ by $E_T(30)$ for the former principle, and the hydrogen bonding capability of the solvent as a criterion in the latter case.[12] Topological studies by FE-SEM and AFM also well reflect this situation (Figure S6). The mixture state of 2-dimensional **D1** crystals and 1-dimensional fibril supramolecular structures of **A1** is clearly manifested when SVA is carried out with polar aprotic solvent (MeCN) vapor (Figure S6c,d); however, bulk CT domains are immediately recovered by nonpolar (DCE) SVA (Figure S6e,f).

As well as the luminescence switching behavior by polarity-and proticity-dependent SVA (see entries ii and iii of Figure 6), the mixed CT phase can be triggered by thermal/

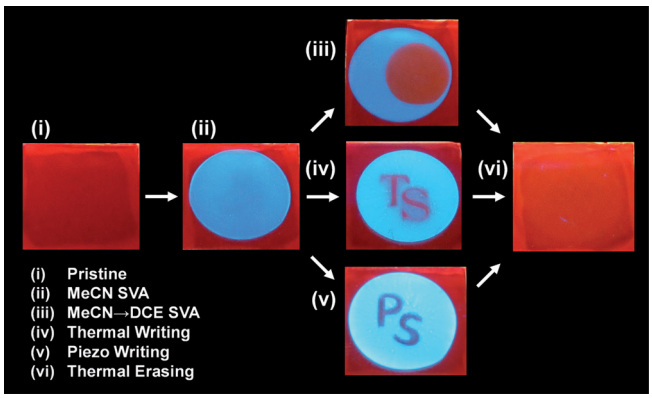

Figure 6. Optical memory demonstration of **D1**-**A1** CT spin-coated film consisting of three components (**D1**, **A1**, and PMMA), utilizing various external stimuli. The thermal erasing process that took place after piezo writing exhibited an inevitable stain.

mechanical stimuli, which enables us to design a multistimuli-responsive programmable fluorescence memory system (Figure 6). As depicted in entries iv and v of Figure 6, thermal and piezo writing on the blue emissive film indeed result in a red emission by mixed-phase formation. This thermal (mechanical) stimulus-induced phase transition can be attained by overcoming the activation energy to form the thermodynamically favorable CT (mixed) phase by the diffusion of the thermally (mechanically) activated mobile **D1** molecules to the **A1** lattice (see the Supporting Information, Figure S7 for DSC analyses).

In summary, we have successfully demonstrated stimuli-responsive reversible PL switching (red↔blue) by introducing a noncentrosymmetric acceptor to form a reconfigurable CT complex system. This PL switching approach provides an intuitive way of controlling optical properties by facile phase alteration, whose emission energy is highly predictable from frontier MOs of the constituent D/A molecules. Furthermore, we believe the molecular design rationale and crystal engineering strategy reported here might not only provide important insights for the supramolecular control of intermolecular interactions by the strategic selection of external triggers, but might also engender inspiration for controlling the nanostructure and/or phases of D-A heterosystems.

Acknowledgements

This research was supported by the National Research Foundation of Korea (NRF) through a grant funded by the Korea government (MSIP; No. 2009-0081571). The work at IMDEA was supported by the Spanish Ministerio de Economía y Competitividad (MINECO; project CTQ2014-58801), and by the Campus of International Excellence (CEI) UAM + CSIC.

Keywords: charge-transfer complex · fluorescence switching · self-assembly · supramolecular chemistry

How to cite: *Angew. Chem. Int. Ed.* **2016**, *55*, 203–207
Angew. Chem. **2016**, *128*, 211–215

[1] a) Y. Sagara, T. Kato, *Nat. Chem.* **2009**, *1*, 605; b) S.-J. Yoon, J. W. Chung, J. Gierschner, K. S. Kim, M.-G. Choi, D. Kim, S. Y. Park, *J. Am. Chem. Soc.* **2010**, *132*, 13675; c) H. Ito, M. Muromoto, S. Kurenuma, S. Ishizaka, N. Kitamura, H. Sato, T. Seki, *Nat. Commun.* **2013**, DOI: 10.1038/ncomms3009; d) P. Galer, R. C. Korošec, M. Vidmar, B. Šket, *J. Am. Chem. Soc.* **2014**, *136*, 7383; e) G. Fan, D. Yan, *Sci. Rep.* **2014**, *4*, 4933; f) D. Yan, H. Yang, Q. Meng, H. Lin, M. Wei, *Adv. Funct. Mater.* **2014**, *24*, 587; g) X. Luo, J. Li, C. Li, L. Heng, Y. Q. Dong, Z. Liu, Z. Bo, B. Z. Tang, *Adv. Mater.* **2011**, *23*, 3261; h) T. Mutai, H. Tomoda, T. Ohkawa, Y. Yabe, K. Araki, *Angew. Chem. Int. Ed.* **2008**, *47*, 9522; *Angew. Chem.* **2008**, *120*, 9664.

[2] A. Das, S. Ghosh, *Angew. Chem. Int. Ed.* **2014**, *53*, 2038; *Angew. Chem.* **2014**, *126*, 2068.

[3] a) M. S. Kwon, J. Gierschner, S.-J. Yoon, S. Y. Park, *Adv. Mater.* **2012**, *24*, 5487; b) M. S. Kwon, J. Gierschner, J. Seo, S. Y. Park, *J. Mater. Chem. C* **2014**, *2*, 2552; c) J. Luo, L.-Y. Li, Y. Song, J. Pei, *Chem. Eur. J.* **2011**, *17*, 10515; d) G. Liu, J. Liu, Y. Liu, X. Tao, *J. Am. Chem. Soc.* **2014**, *136*, 590; e) A. Das, M. R. Molla, A. Banerjee, A. Paul, S. Ghosh, *Chem. Eur. J.* **2011**, *17*, 6061; f) A. Das, M. R. Molla, B. Maity, D. Koley, S. Ghosh, *Chem. Eur. J.* **2012**, *18*, 9849; g) J. S. Park, K. Y. Yoon, D. S. Kim, V. M. Lynch, C. W. Bielawski, K. P. Johnston, J. L. Sessler, *Proc. Natl. Acad. Sci. USA* **2011**, *108*, 20913.

[4] a) C. Wang, S. Yin, S. Chen, H. Xu, Z. Wang, X. Zhang, *Angew. Chem. Int. Ed.* **2008**, *47*, 9049; *Angew. Chem.* **2008**, *120*, 9189; b) C. Wang, Y. Guo, Y. Wang, H. Xu, R. Wang, X. Zhang, *Angew. Chem. Int. Ed.* **2009**, *48*, 8962; *Angew. Chem.* **2009**, *121*, 9124; c) K. V. Rao, K. Jayaramulu, T. K. Maji, S. J. George, *Angew. Chem. Int. Ed.* **2010**, *49*, 4218; *Angew. Chem.* **2010**, *122*, 4314.

[5] a) J.-Y. Wang, J. Yan, L. Ding, Y. Ma, J. Pei, *Adv. Funct. Mater.* **2009**, *19*, 1746; b) Y. L. Lei, L. S. Liao, S. T. Lee, *J. Am. Chem. Soc.* **2013**, *135*, 3744; c) W. Zhu, R. Zheng, X. Fu, H. Fu, Q. Shi, Y. Zhen, H. Dong, W. Hu, *Angew. Chem. Int. Ed.* **2015**, *54*, 6785.

[6] a) S. K. Park, S. Varghese, J. H. Kim, S.-J. Yoon, O. K. Kwon, B.-K. An, J. Gierschner, S. Y. Park, *J. Am. Chem. Soc.* **2013**, *135*, 4757; b) M. Wykes, S. K. Park, S. Bhattacharyya, S. Varghese, J.

E. Kwon, D. R. Whang, I. Cho, R. Wannemacher, L. Lüer, S. Y. Park, J. Gierschner, *J. Phys, Chem. Lett.* **2015**, *6*, 3682.
[7] M. M. Safont-Sempere, G. Fernández, F. Würthner, *Chem. Rev.* **2011**, *111*, 5784.
[8] a) B.-K. An, S. H. Gihm, J. W. Chung, C. R. Park, S.-K. Kwon, S. Y. Park, *J. Am. Chem. Soc.* **2009**, *131*, 3950; b) J. H. Kim, J. W. Chung, Y. Jung, S.-J. Yoon, B.-K. An, H. S. Huh, O. W. Lee, S. Y. Park, *J. Mater. Chem.* **2010**, *20*, 10103.
[9] Crystal data for **D1**-**A1** mixed CT: red crystal, $0.23\times0.20\times0.13\,mm^3$, trichlinic, $P\bar{1}$, $a=10.9520(3)$, $b=14.4295(4)$, $c=15.9432(4)$ Å, $\alpha=89.667(2)$, $\beta=77.845(2)$, $\gamma=70.3940(10)°$, $V=2314.49(11)$ Å^3, $Z=2$, $\rho_{calcd}=1.430\,mg\,m^{-3}$, $\mu=0.216\,mm^{-1}$, $2\theta_{max}=27.49°$, independent reflections 10596 ($R_{int}=0.0446$), final R indices ($I>2\sigma(I)$ $R1=0.0943$, $\omega R2=0.2768$), R indices (all data, $R1=0.1374$, $\omega R2=0.3197$), largest diffusion peak and hole: 1.015 and $-1.574\,e\,Å^{-3}$, APEX II detector, λ ($Mo_{K\alpha}$, 0.71073 Å), $T=173$ K, refinement method of full-matrix least-squares on F^2 (goodness-of-fit on $F^2=1.052$), data (10596)/restraints (0)/parameters (626). The diffraction result exhibited 1:1 stoichiometry of **D1**:**A1**. The residual electron density implied solvent inclusion, which was further characterized by TGA and NMR. However, precise picture of such solvent inclusion could not be drawn owing to the disorder in solvent. The reasonable structure, however, was extracted by placing reduced solvent molecule, C-Cl, according with bond length of 1.7 Å found during simulation procedure. CCDC 1421282 contain the supplementary crystallographic data for this paper. These data can be obtained free of charge from The Cambridge Crystallographic Data Centre.
[10] C. Reichardt in *Solvents and Solvent effects in Organic Chemistry*, 3rd ed., Wiley-VCH, Weinheim, **2003**, pp. 411 – 443.
[11] Solvent abbreviation list: Ether: diethyl ether, DCM: dichloromethane, DCE: 1,2-dichloroethane, ACT: acetone, DMSO: dimethyl sulfoxide, MeCN: acetonitrile, IPA: isopropyl alcohol, EtOH: ethanol, MeOH: methanol.
[12] G. A. Breault, C. A. Hunter, P. C. Mayers, *J. Am. Chem. Soc.* **1998**, *120*, 3402.
[13] R. Foster, *J. Am. Chem. Soc.* **1960**, *82*, 1075.
[14] M. S. Cubberley, B. L. Iverson, *J. Am. Chem. Soc.* **2001**, *123*, 7560.

Received: September 2, 2015
Published online: November 20, 2015

